Supporting Information

Sulfur Vacancy induced Co_3S_4@$CoMo_2S_4$ nanocomposite as functional electrode for high performance Supercapacitor.

Njemuwa Nwaji[a], Hyojin Kang[b], Mahedra Goddati[b], Lemma Teshome Tufa[a], Juyoung Gwak [b], Abhishek Sharan[c], Nirpendra Singh*[c, d], Jaebeom Le*[a, b]

Material characterization

The morphology of all prepared materials was investigated by field emission scanning electron microscopy (FE-SEM, SU8000, Hitachi, Japan) and transmission electron microscopy (JEM-2100F, JEOL Ltd., Tokyo, Japan). The crystal structures of these materials were determined with an X-ray diffractometer (XRD, Empyrean series-2; PANalytical, Netherlands) with Cu Kα radiation (λ =1.5410 nm) over the 2θ range of 10 ~ 90° at 40 kV, 40 mA. Material composition and surface electronic characterization were done using XPS with K-α XPS (Thermo Scientific). N_2 adsorption-desorption isotherms were recorded with a surface area and porosity analyzer (Micromeritics 2020, ASAP, USA).

Computational Details

The theoretical investigation of K and OH adsorption on CoMo2S4 nanocomposite is based on density functional theory calculations as implemented in the Vienna ab-initio Simulation package (VASP) [1,2], using Generalized Gradient Approximation of Perdew, Burke, and Ernzerhof [3] as the exchange-correlation functional. The interactions between valence electrons and ionic cores are treated using the projector-augmented-wave potentials [4,5]. Monoclinic unit cell of $CoMo_2S_4$ with a = b = 6.40 Å, and c = 5.94 Å is used for the analysis. K and OH adsorption on (100) surface of $CoMo_2S_4$, Fe doped $CoMo_2S_4$, and Fe doped $CoMo_2S_{4-x}$ is performed for comparison. Our calculations reveal that substitutional Fe doping on the Co site is energetically more favorable than on Mo site. Sulphur vacancy on (100) surface is introduced for adsorption analysis in $CoMo_2S_{4-x}$. A vacuum region of 15 Å is used in the supercell containing the surface to avoid spurious

interaction with the periodic images. Spin-polarized calculations with energy cutoff of 540 eV is used for plane wave basis set expansion. Γ-centered k-point mesh of 1x3x3 is adopted for calculations to sample the Brillouin zone of the supercell calculations containing vacuum. For supercell relaxations, only two layers near the vacuum are relaxed, while rest of the atoms far from the surface are kept fixed. For K and OH adsorption different surface sites are tested, and the one with minimum energy is taken for comparison. Density of states calculations are performed on a finer Γ-centered mesh of 1x6x6.

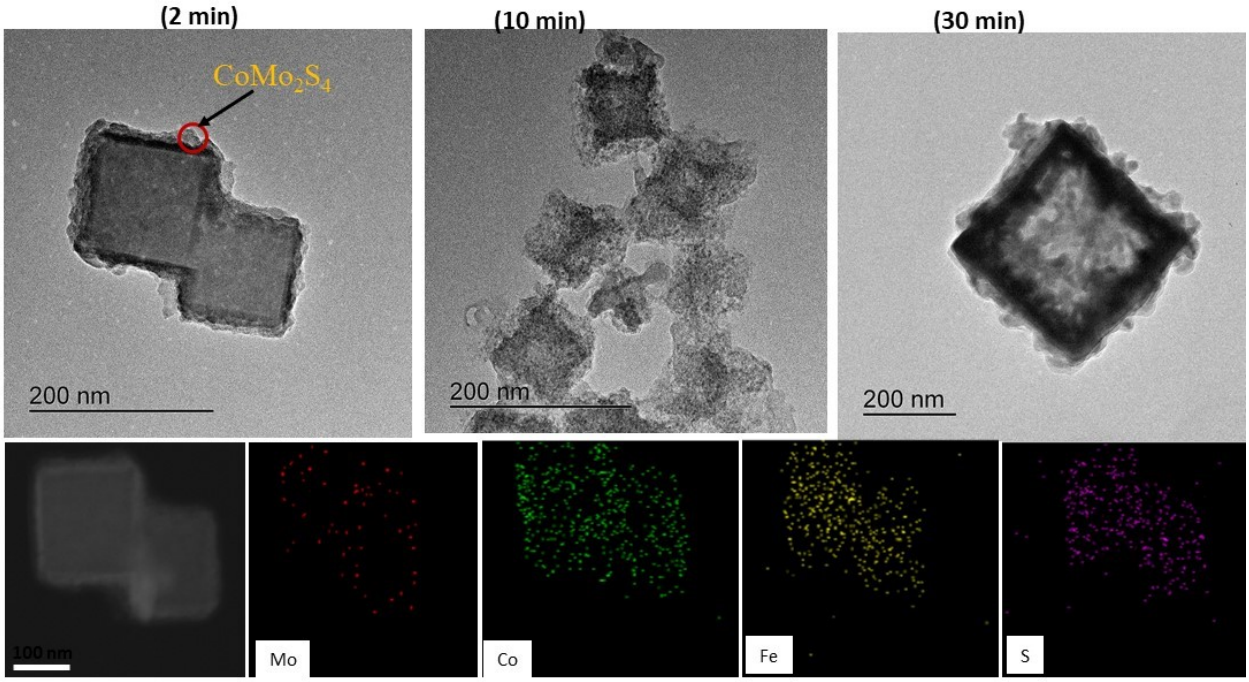

Figure S1. Time images of aliquot portion of the sulfurization reaction to form Fe-Co_3S_4@$CoMo_2S_4$ (upper) and the elemental mapping of the product formed after 2 minutes of reaction.

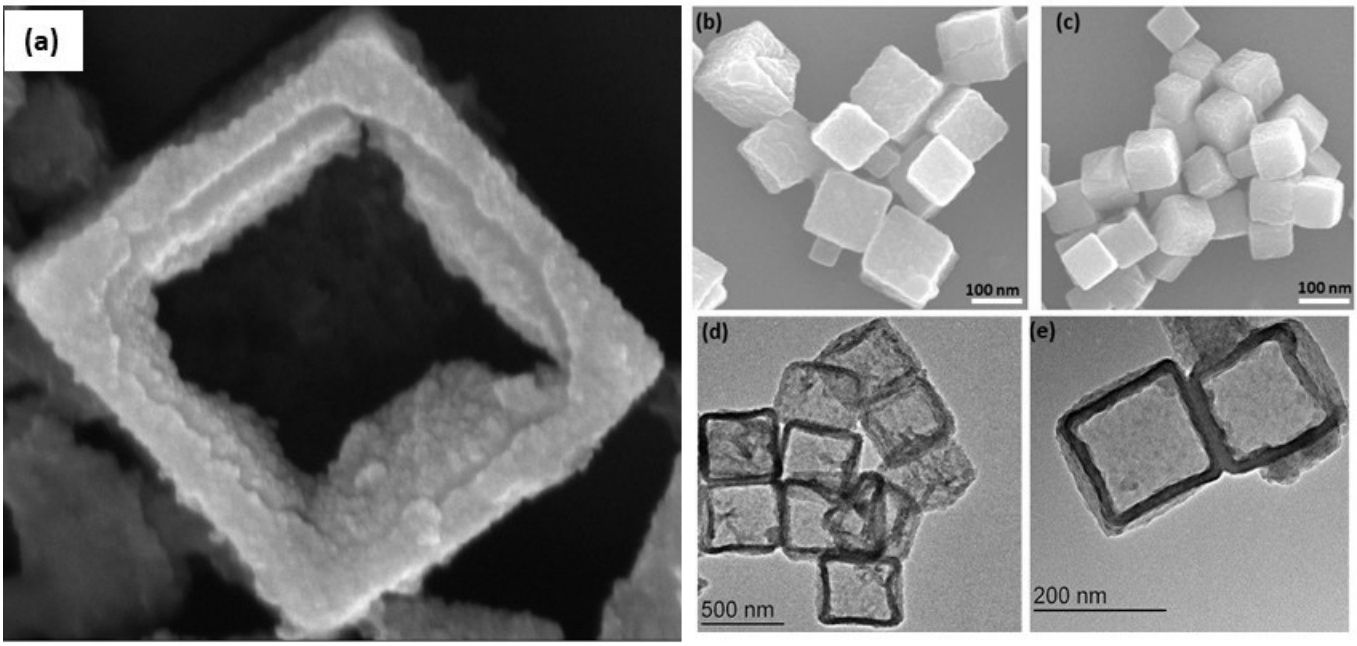

Figure S2. (a, b) SEM images of Co-ZIF doped with 0.03 and 0.06 mmol concentration of Fe, (c) TEM image of hollow Fe-doped Co_3S_4@$CoMoS_4$ and (d) TEM image of hollow Co_3S_4@$CoMoS_4$

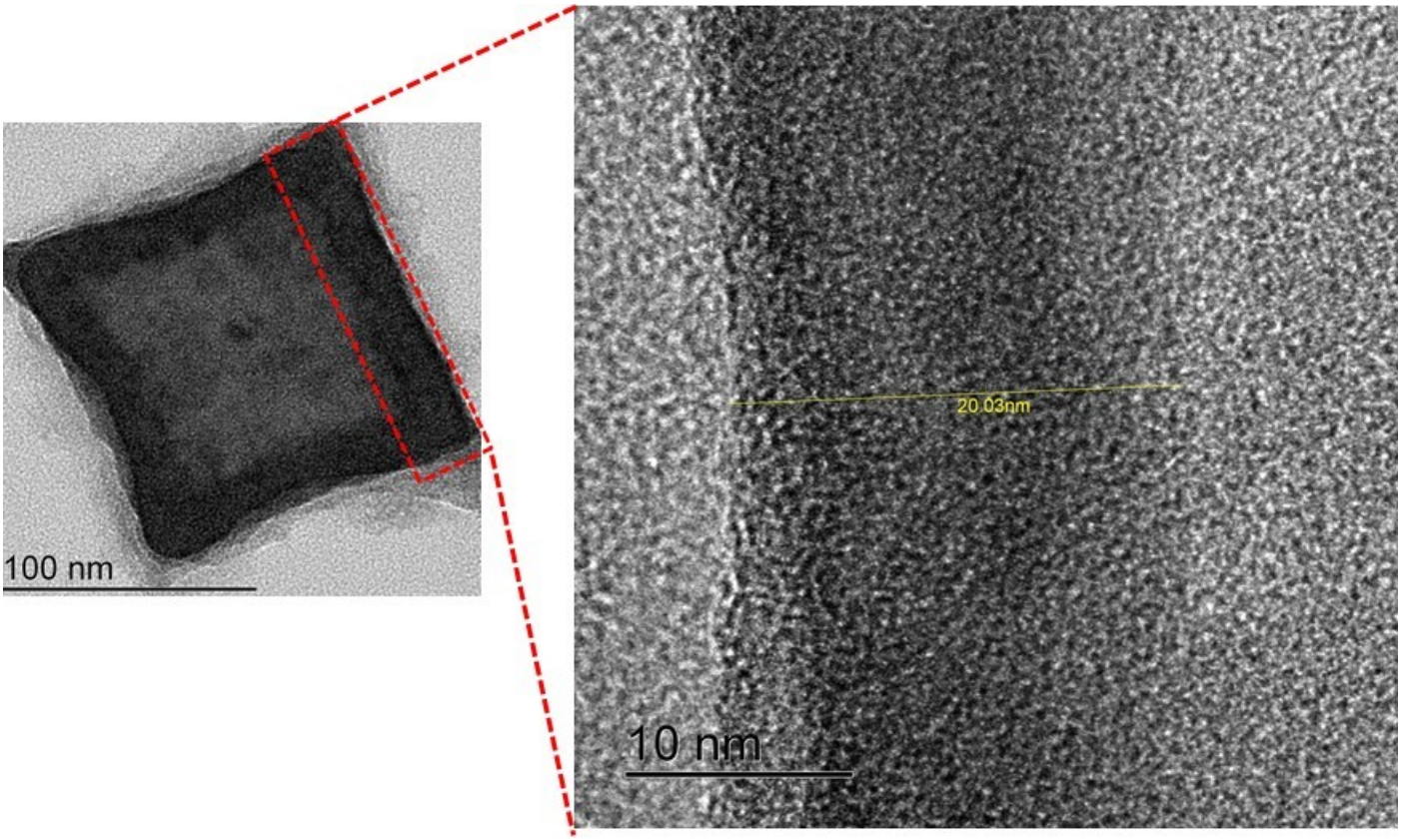

Figure S3: Low and High magnification TEM image of $FeCo_3S_4$@$CoMoS_4$ showing the shell thickness

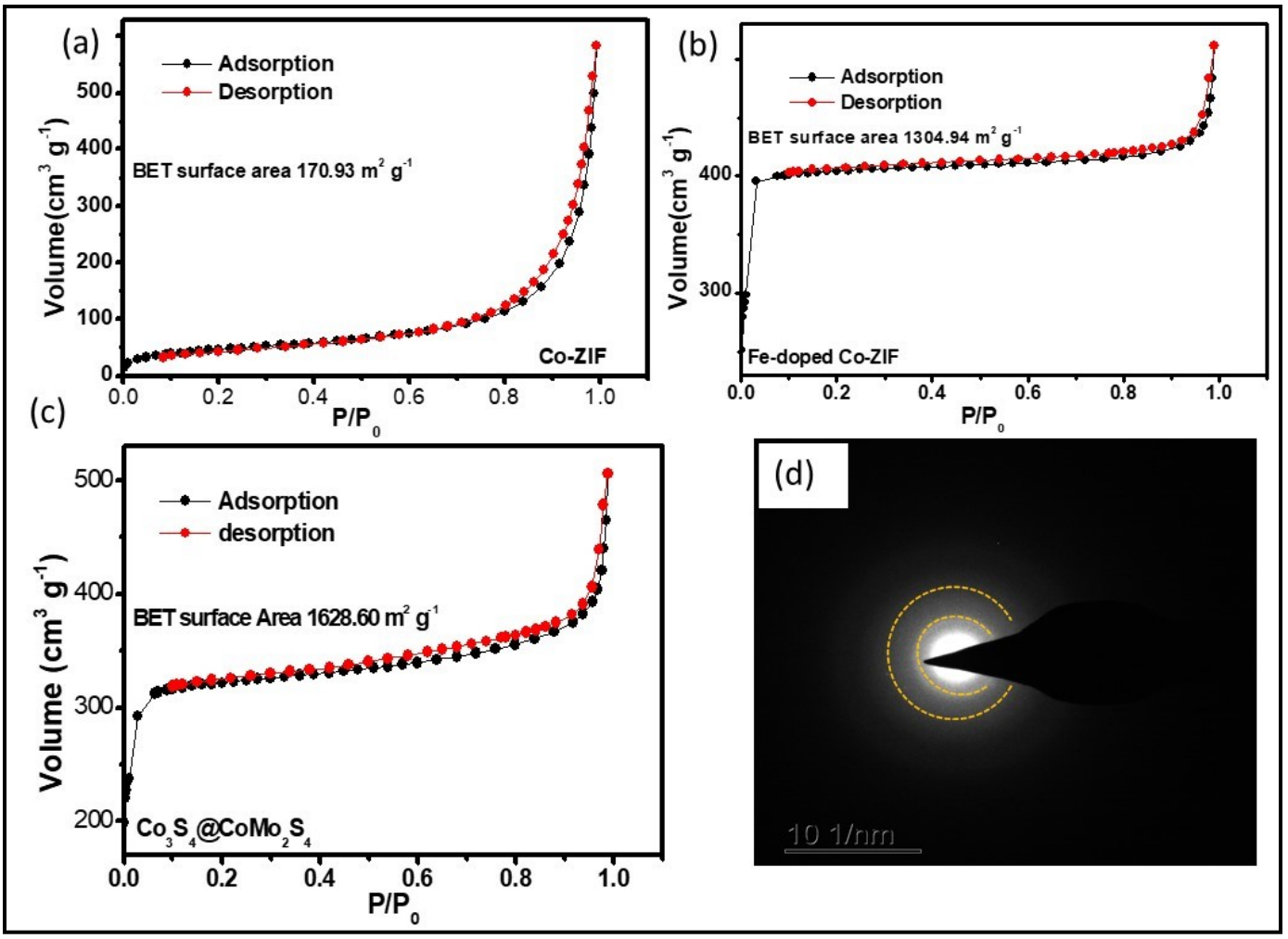

Figure S4 (a-c). N_2-adsorption/desorption isotherms and (d) SAED of $FeCo_3S_4$@$CoMoS_4$ showing the polycrystalline nature.

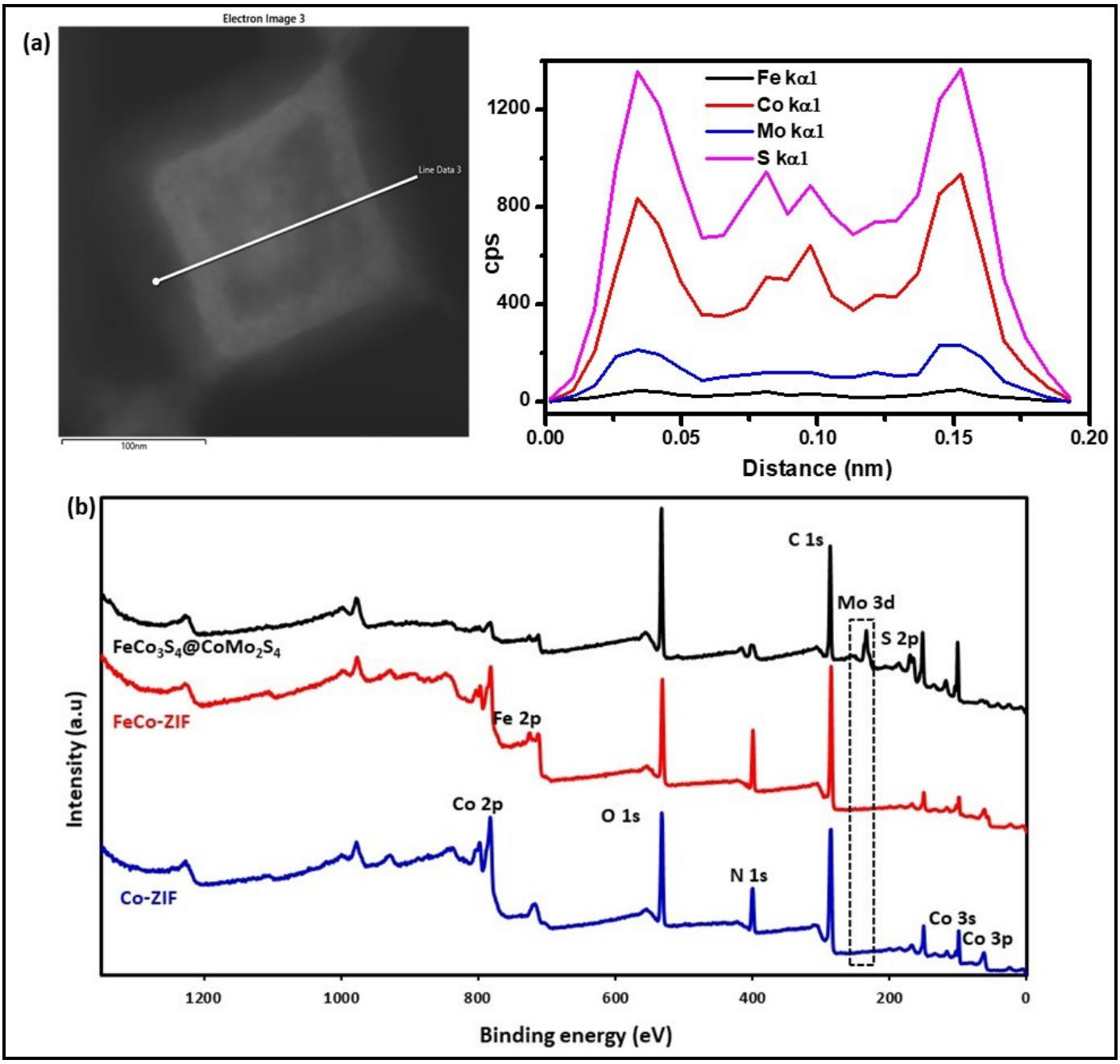

Figure S5. (a)Representative elemental line scanning profiles of $FeCo_3S_4$@$CoMoS_4$ (b) XPS Survey spectra of the as prepared materials.

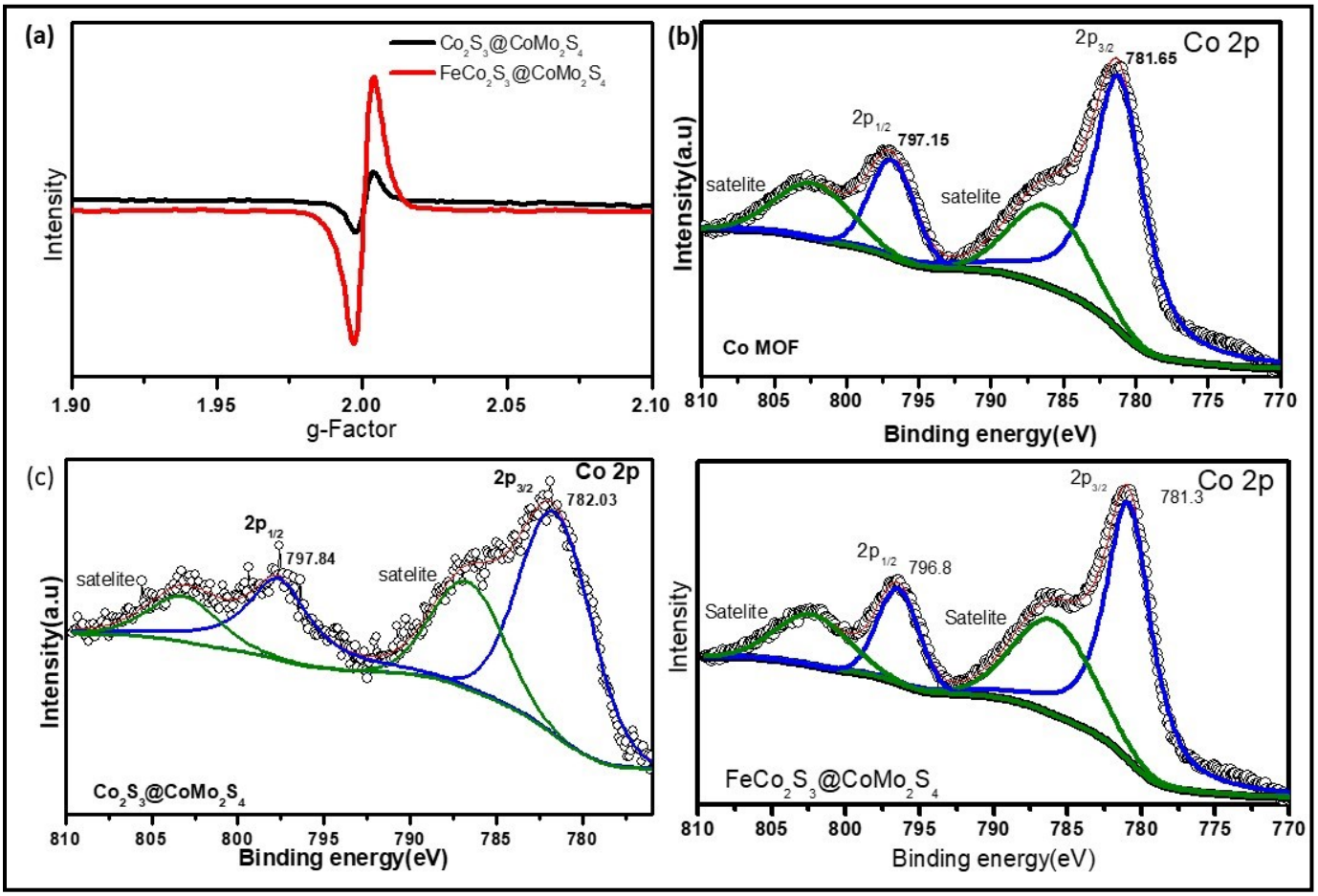

Figure S6: EPR spectra (a) and high resolution XPS (b, c, d) of the as prepared nanostructures

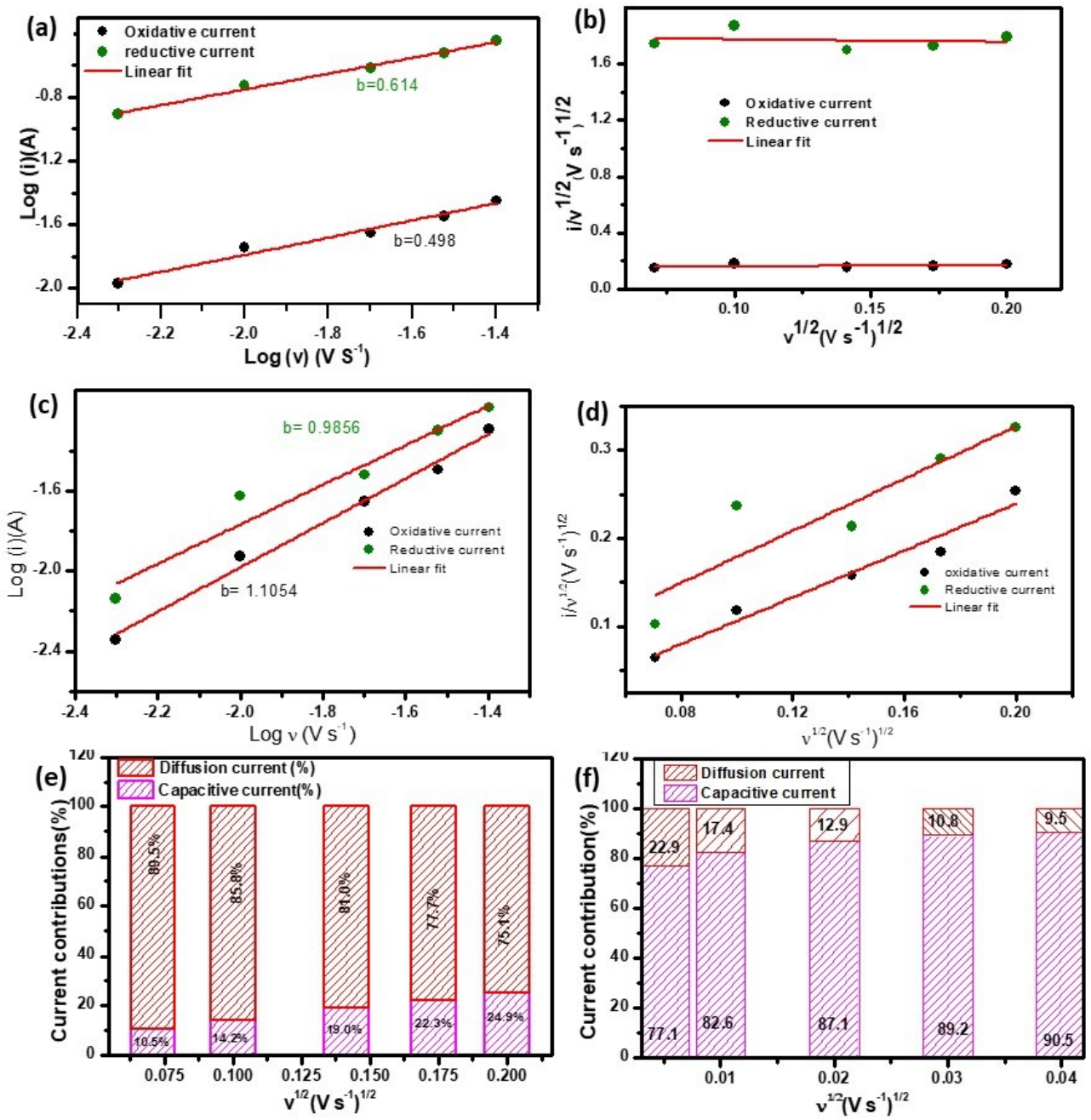

Figure S7: The power's law and modified power law plots for (a, b) $Fe_{0.9}Co$-MOF, (c, d) $FeCo_2S_3@CoMo_2S_4$ and the corresponding charge storage mechanism.

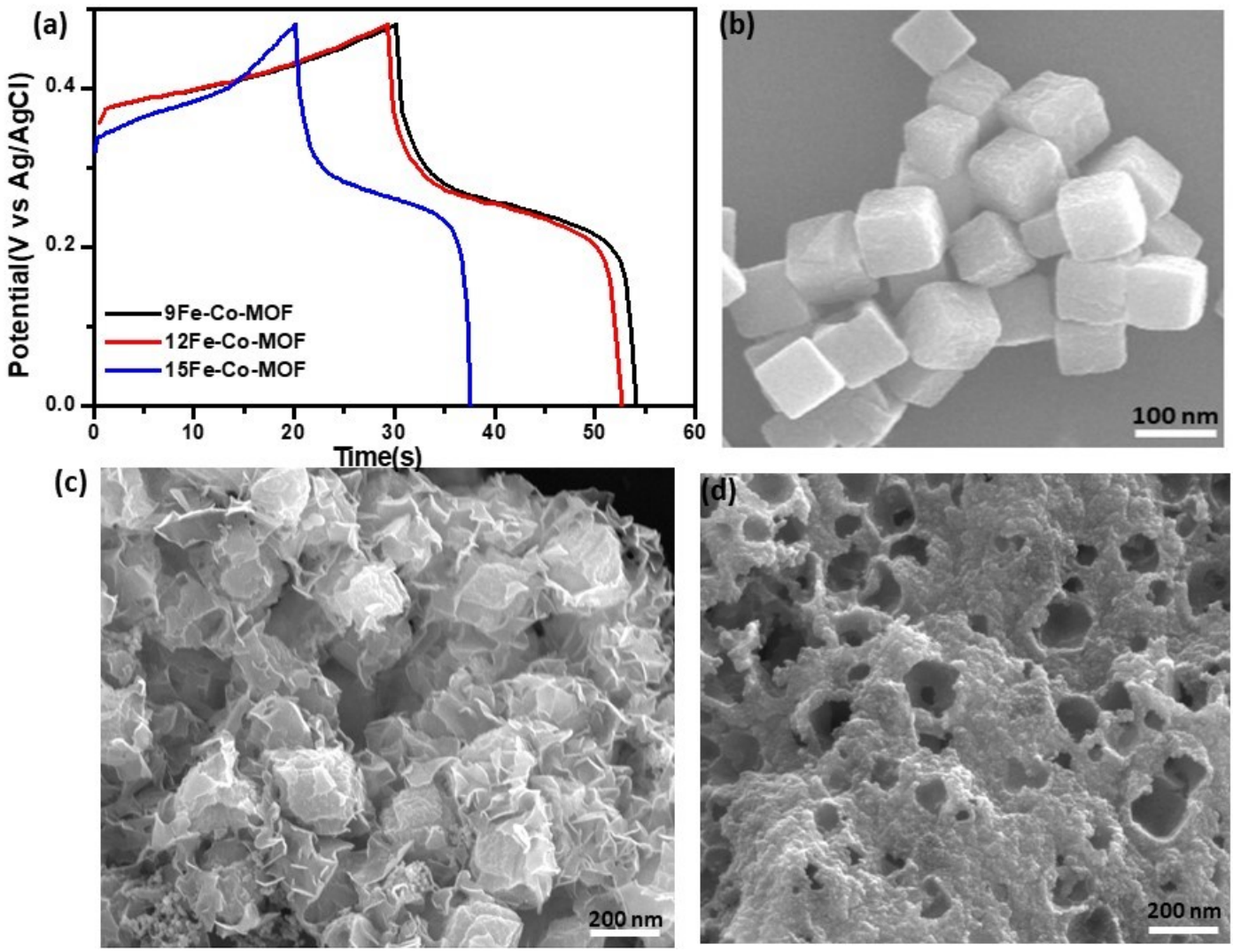

Figure S8. GCD Curve (a) and SEM images (b-c) of Co-MOF doped with 0.09, 0.12 and 0.15 mmol concentration of Fe

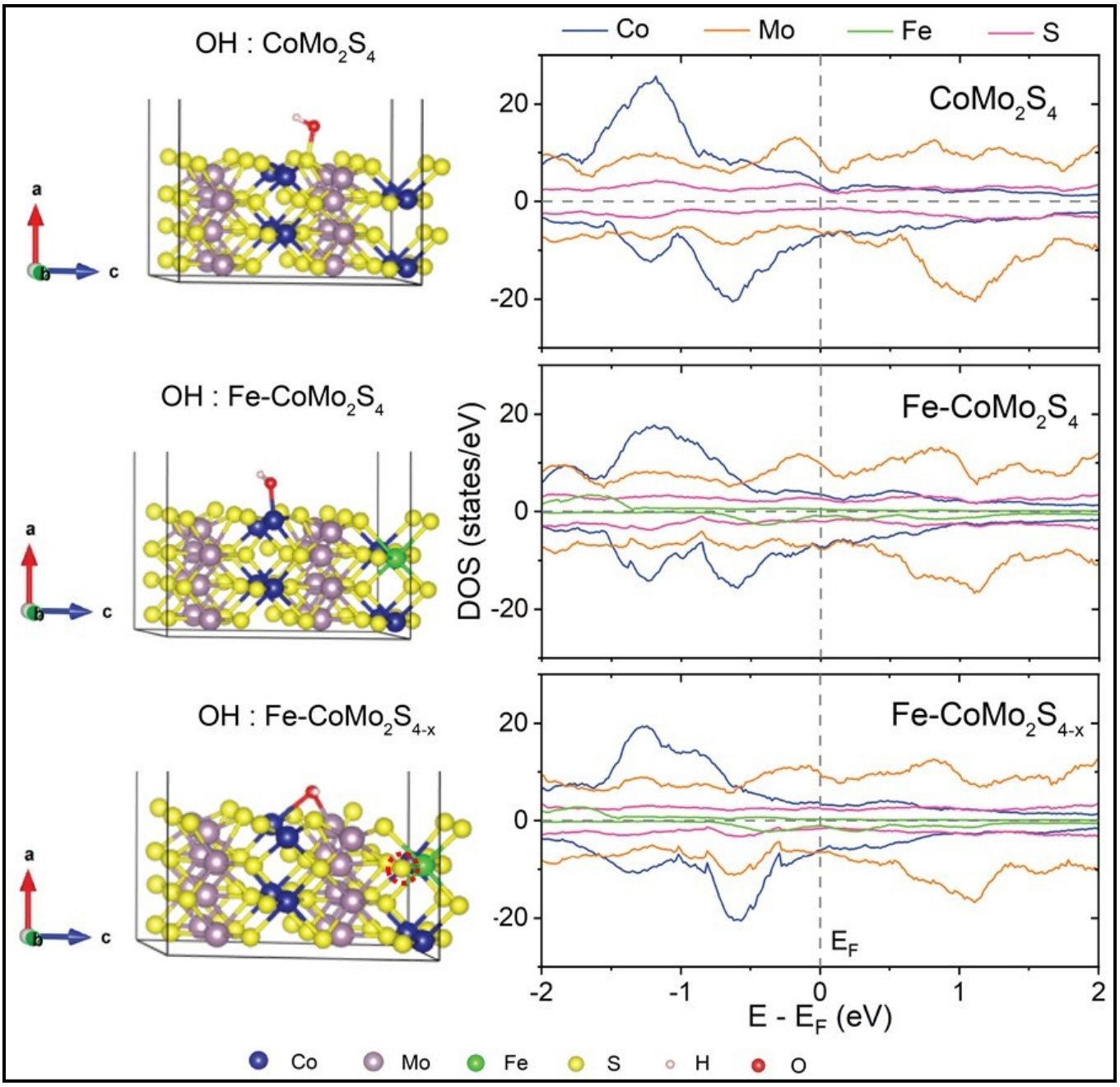

Figure S9: Optimized structures of the undoped and Fe-doped CoMo2S4 shell and the corresponding densities of states

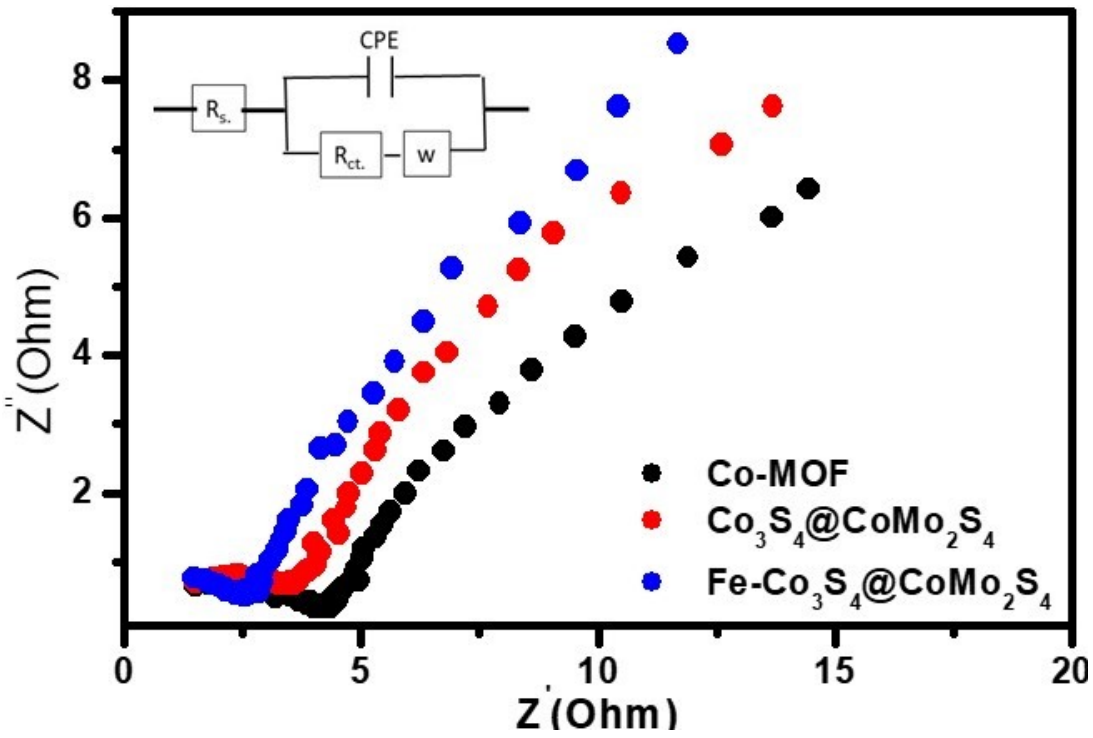

Figure S10. EIS Nyquist plots for the as prepared electrode materials.

Table S1. Comparison of electrochemical performance of reported electrode material

Electrode Material	Specific capacitance ($F\ g^{-1}$)	Rate performance (Fg^{-1})	Cycle stability	Ref.
Co-Ni-B-S	1281 at 1 A g^{-1}	802.9 at15 A g^{-1}	92.1% at 15 A g^{-1} 10 000 cycles	6
Fe-NiCo-S	1919.6 at 1 A g^{-1}	1122.0 at 10 A g^{-1}	78.0% at 10A g^{-1} 5000 cycles	7
NiS@CoS	1210 at 1 A g^{-1}	990 at 10 A g^{-1}	80.94% at 10 A g^{-1} 2000 cycles	8
NiCo-MOF	1109 at 0.5 A g^{-1}	957 at 10 A g^{-1}	81.4% at 10 A g^{-1} 5000 cycles	9
$Ni_xCo_{3-x}S_4$	895.2 at 1 A g^{-1}	585.2 at 20 A g^{-1}	79.4% at 5 A g^{-1} 1500 cycles	10
Co_9S_8/NF nanoarrays	1090 at 0.5 A g^{-1}	600.3 at 10 A g^{-1}	87.4% at 10A g^{-1} 10000 cycles	11
Fe-Co_3S4@$CoMo_2S_4$	970.8 at 1 A g^{-1}	393.5 at 20 A g^{-1}	96.5% at 10A g^{-1} 6000 cycles	This work

Reference:

1. Kresse, G.; Furthmüller, J. Efficient Iterative Schemes for Ab Initio Total-Energy Calculations Using a Plane-Wave Basis Set. Phys. Rev. B 1996, 54 (16), 11169.
2. Kresse, G.; Furthmüller, J. Efficiency of Ab-Initio Total Energy Calculations for Metals and Semiconductors Using a Plane-Wave Basis Set. Comput. Mater. Sci. 1996, 6 (1), 15–50.
3. Perdew, J. P.; Burke, K.; Ernzerhof, M. Generalized Gradient Approximation Made Simple. Phys. Rev. Lett. 1996, 77 (18), 3865–3868.
4. Bl¨ochl, P. E. Projector augmented-wave method, Phys.Rev. B 1994, 50, 17953.
5. Kresse, G.; Joubert, D. From ultrasoft pseudopotentials to the projector augmented-wave method, Phys.Rev. B 1999, 59, 1758.
6. Wang, Q.; Luo, Y.; Hou, R.; Zaman, S.; Qi, K.; Liu, H.; Park, H. S.; Xia, B. Y. Redox Tuning in Crystalline and Electronic Structure of Bimetal-Organic Frameworks Derived Cobalt/Nickel Boride/Sulfide for Boosted Faradaic Capacitance. Adv. Mater. 2019, 31, 1905744-1905752.
7. Liu, R.; Xu, S.; Shao, X.; Wen, Y.; Shi, X.; Shi, X.; Huang, L.; Hong, M.; Hu, J.; Yang, Z. Defect-Engineered NiCo-S Composite as a Bifunctional Electrode for High-Performance Supercapacitor and Electrocatalysis. ACS Appl. Mater. Interfaces, 2021, 13, 47717-47727
8. Miao, Y.; Zhang, X.; Zhan, J.; Sui, Y.; Qi, J.; Wei, F.; Meng, Q.; He, Y.; Ren, Y.; Zhan, Z.; Sun, Z. Hierarchical NiS@CoS with Controllable Core-Shell Structure by Two-Step Strategy for Supercapacitor Electrodes, Adv. Mater. Interfaces, 2019, 7, 1901618
9. Liu, Y.; Wang, Y.; Chen, Y.; Wang, C.; Guo, L. NiCo-MOF Nanosheets Wrapping Polypyrrole Nanotubes for High-Performance Supercapacitors. Appl. Surf. Sci. 2020, 507, 145089-145097.
10. Yu, L.; Zhang, L.; Wu, H. B.; Lou, X. W. Formation of $Ni_{(x)}Co_{(3-x)}S_{(4)}$ Hollow Nanoprisms with Enhanced Pseudocapacitive Properties. Angew. Chem. Int. Ed. 2014, 53, 3711-3714.
11. Han, X.; Tao, K.; Wang, D.; Han, L. Design of a Porous Cobalt Sulfide Nanosheet Array on Ni Foam from Zeolitic Imidazolate Frameworks as an Advanced Electrode for Supercapacitors. Nanoscale 2018, 10, 2735– 2741